Supporting information for

# Nanostructured Ir-supported on $Ti_4O_7$ as cost effective anode for proton exchange membrane (PEM) electrolysis

Li Wang,[a] Philipp Lettenmeier,[a] Ute Golla-Schindler,[b] Pawel Gazdzicki,[a] Natalia A. Cañas,[a] Tobias Morawietz,[c] Renate Hiesgen,[c] S. Schwan Hosseiny,[a] Aldo S. Gago*[a] and K. Andreas Friedrich[a,d]

[a]Institute of Engineering Thermodynamics, German Aerospace Center, Pfaffenwaldring 38-40, Stuttgart, 70569, Germany

[b]Central Facility of Electron Microscopy, University of Ulm, Helmholtzstr. 18, Ulm, 89081, Germany

[c]University of Applied Sciences Esslingen, Dep. of Basic Science, Kanalstrasse 33, Esslingen, 73728, Germany

[d]Institute of Energy Storage, University of Stuttgart, Stuttgart, 70550, Germany

*E-mail address: aldo.gago@dlr.de (A. S. Gago).

## Experimental

### BET measurements:

The specific surface area for $Ti_4O_7$ and $Ir/Ti_4O_7$ powders was determined by Brunauer-Emmett-Teller (BET) method using nitrogen adsorption isotherm obtained at 77 k (Sorptomatic 1990, Porotec).

### pH measurements:

For pH measurements, the pH meter HI 255 Combined Meter pH/mV EX/TDS/NaCl (HANNA Instruments) was used. Before the measurements a three-point calibration was executed using buffering solutions with a pH-value of 7.01, 4.01 and 9.18.

Four powders ($Ti_4O_7$, $TiO_2$, Ir black and $Ir/Ti_4O_7$) were used for pH determination. For each powder three suspension samples have been prepared. In each case, 15 mg of powder was dispersed in 15 ml of deionized water and homogenized for five minutes in an ultrasonic bath.

For measuring the pH-value, a pH-electrode (type: HI 1131) as well as a temperature electrode were used and immersed into the suspension until the measuring value got constant. In doing so, pH-values and the temperature of three suspensions for each powder were determined and were averaged for the final pH value.

**Zeta potential measurements**

0.1 wt. % of the samples ($Ti_4O_7$, $TiO_2$ and Ir black powders) were dispersed in deionized water to form a homogeneous suspension. For the zeta potential measurements, a Stabino particle charge mapping system was used. First, the Zeta potential was recorded against time while monitoring pH, temperature and conductivity. Afterwards, $KNO_3$ was added to the suspension until 10 mM $KNO_3$ concentration was achieved to provide a constant conductivity. The titration was carried out with 0.01 M $HNO_3$ ($Ti_4O_7$ and Ir black) / 0.01 M KOH ($TiO_2$) every 30 seconds to find the point of zero charge.

**Electrochemical measurements protocol before and after XPS analysis**

With respect to XPS analysis on both catalysts before and after electrochemical measurements, Ir/$Ti_4O_7$ and Ir Black inks were casted on four gold plates (two plates for each), drying in Ar atmosphere. One group of samples was sent to XPS analysis directly, while another group of them were applied with following electrochemical protocols before they were analyzed by XPS. Three scans of cyclic voltammetry (CV) from 1.0 V to 1.6 V vs. RHE with a scan rate of 5 mV $s^{-1}$ were used to check the OER activity, further 50 cycles of CV between 0.05 V to 1.5 V were carried out at 500 mV $s^{-1}$, at the end, three scans of CV from 0.4 V to 1.4 V were performed at a scan rate of 20 mV $s^{-1}$.

**Electrochemical measurements on gold rotating disk electrode (Au-RDE)**

Regarding to all the electrochemical measurements with Au-RDE, the same catalytic ink was used, 4 μL of the suspension was pipetted onto the surface of a gold rotating disc electrode (Au-RDE, Pine instruments) of 0.196 $cm^2$. Before preparing the catalyst-modified electrode, the same cleaning steps as for GC-RDE were applied for Au-RDE. Pure Ar or $O_2$ (purity 5.0, Linde) was bubbled into the electrolyte for 30 minutes before cyclic voltammetry (CV) and linear scan voltammetry (LSV). In this case, all the measurements were performed at room temperature.

**CO stripping measurements:**

The study on electrochemically active surface sites was carried out by CO-stripping technique. New catalyst modified GC-RDE was prepared and applied the following steps. Firstly, the electrolyte solution was purged with CO for 10 minutes, followed by a chronoamperometry at 0.05 V *vs.* RHE for 10 minutes. Afterwards the CO gas was again changed to Ar, after saturating the solution with Ar for another 10 minutes, three cycles of CV with a scanning rate of 50 mV $s^{-1}$ from 0.05 V to 1.20 V vs. RHE were performed to fully oxidize the adsorbed CO molecules on the surface of the catalytic layers.

**Accessible active sites determination (Redox peak determination)**

The redox peak of $Ir^{3+} \leftrightarrow Ir^{4+}$ was used for determining accessible active sites for both catalysts [1,2], a newly prepared GC-RDE modified with catalyst was immersed in Ar-saturated electrolyte. Three CVs were performed from 1.0 V to 1.6 V in order to check working condition of as-prepared electrode, afterwards, 50 cycles of CV with a sweep rate of 500 mV $s^{-1}$ between 0.05 V and 1.5 V vs. RHE were applied on the electrode for the pre-electrochemical oxidation of the

catalyst. At the end, the redox peak was determined by 3 cycles of CV from 0.4 to 1.4 V under the scanning rate of 20 mV $s^{-1}$.

## Results and discussion

### 1. X-ray diffraction analysis of Ir/$Ti_4O_7$ powder

The results of the Rietveld analysis for the Ir/ $Ti_4O_7$ powder are presented in Fig. S1. Fitting of the support material was carried out using two main structures: $Ti_4O_7$ (Triclinic, space group (SG): P-1, CIF:1008048) and $K_{1.28}Ti_8O_{16}$ (tetragonal, SG: I4/m, CIF: 2101045). Differences between the measured and fitted spectra were attributed to errors in the fitting of the support material. However, this work was focused on the synthesized nano-sized Ir catalyst and not in the support material (commercially available). Moreover, low values of weighted profile factor (Rwp): 4.85, profile factor (Rp): 3.78 and goodness of fit (GOF): 0.53 were obtained, confirming the refinement quality.

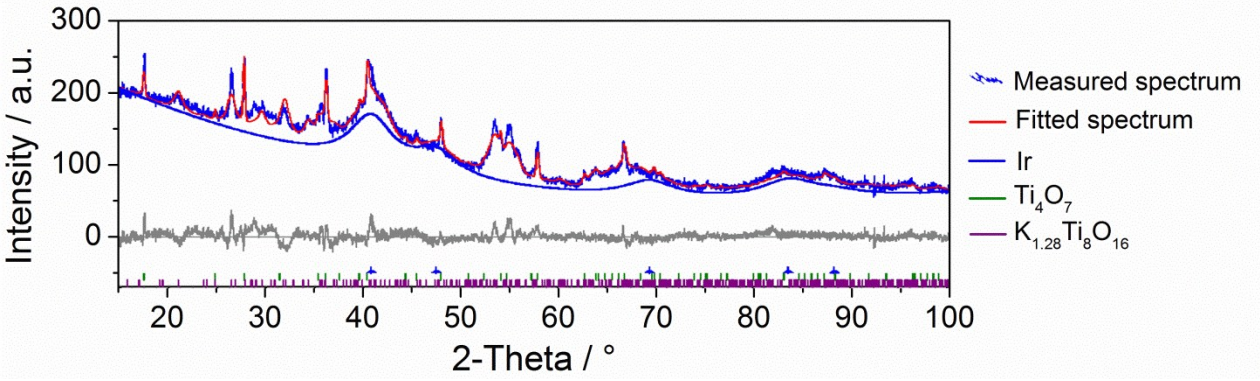


**Fig. S1.** X-ray diffraction pattern and corresponding Rietveld refinement of Ir/$Ti_4O_7$ sample. Ir reflection markers and difference curve are provided on the bottom of the figure.

### 2. XPS analysis of catalyst layer before and after electrochemical treatment

In Fig. S2 Ir composition profiles of pristine Ir/$Ti_4O_7$ and Ir-black (prepared as catalyst layer with Nafion as ionomer) are presented as well as profiles after electrochemical treatment. Apparently, the Ir of the Ir-black sample is initially purely metallic and becomes partially oxidized upon operation especially on the surface (0 – 10 s sputtering); after around 10 s sputtering the Ir-metal fraction stabilizes at around 90% of overall Ir. The Ir-composition profiles of Ir/$Ti_4O_7$ look significantly different, with their surfaces being clearly covered by an oxide layer. Thereby, not only $Ir^{3+}$ has been observed but also a mixed oxide, with the Ir $4f_{7/2}$ level located above 64 eV; the mixed oxide largely vanishes after ~20 s sputtering for the pristine sample; for the electrochemically treated sample the layer is slightly thicker and ~25 s sputtering are needed for its removal. After the surface oxide layers have been removed, it both cases the fraction of metallic Ir is about 65% of the overall Ir signal.

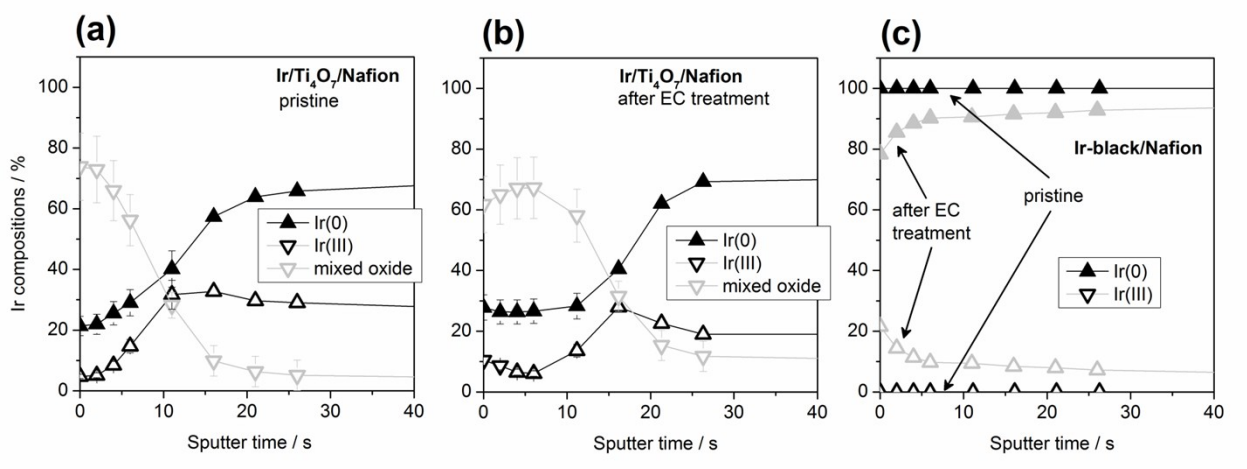


**Fig. S2.** XPS analysis of catalyst layers. (a) and (b) are Ir compositions of $Ir/Ti_4O_7$ before and after electrochemical test, respectively. (c) Ir compositions of Ir/-black before and after electrochemical test.

## 4. AFM analysis on Ir-black catalytic layer

In Fig. S3 (a), a higher magnification of the Ir-black pellet is shown. The Ir particles are identifiable in the adhesion image by a higher adhesion at their boundaries. The crystallite size of the Ir-black was measured in the adhesion image (Fig. S3 (b)) using the Nanoscope Analysis software. In Fig. S3 (c), the evaluated particles are marked in blue. The mean crystallite size was determined to (16.8 ± 0.9) nm in accordance with 16.49 ± 0.04 nm from XRD analysis.

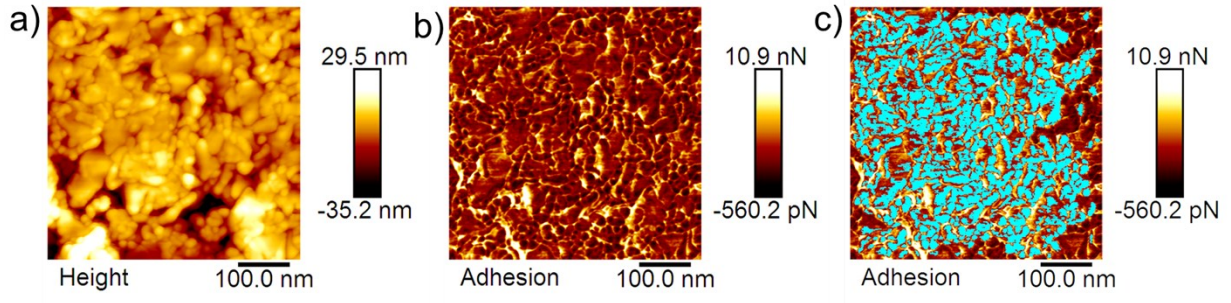


**Fig. S3.** Higher magnification image of the Ir-black pellet surface with (a) topography, (b) adhesion, and (c) particle size analysis with counted particles marked in blue.

## 5. AFM analysis on $Ir/Ti_4O_7$ before and after electrochemical treatment.

PF-KPFM was used to compare the surface potential before and after the electrochemical cycling. All parameters, such as lift height, scan rate, scanned area size, etc., were held constant. Fig. S4 (a) and (b) show PF-KPFM images of $Ir/Ti_4O_7$ before and after the electrochemical treatment. The measured potentials over the whole image are presented in Fig. S4 (c). The potential values are always an average of surface and sub-surface materials. With a higher influence of layers closer to the tip, the observed potential values are higher than for the pure

phases due to their coverage by ionomer. After the electrochemical cycling the potential distribution is much sharper with a maximum at about 1.5 V with respect to the AFM tip. Before the electrochemical measurements, the surface potential had a much wider distribution with a mean value of about 1 V. Before the electrochemical measurements, the surface potential had a much wider distribution with a mean value of about 1 V. The increase in surface potential cannot be explained due to the influence of the different components such as Nafion, $Ti_4O_7$, Ir and $IrO_x$ on the measured potential difference to the tip.

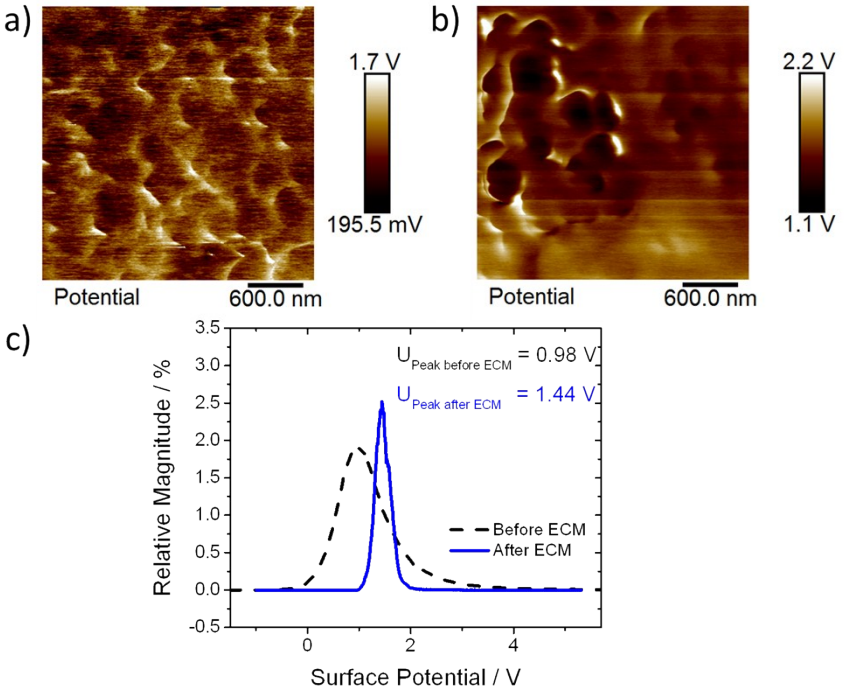


**Fig. S4.** AFM surface potential (KPFM) images of the $Ir/Ti_4O_7$ coated GC electrode containing Nafion ionomer, (a) before, (b) after electrochemical measurements (ECM): 200 cycles cyclic voltammetry between 1.0 and 1.6 V *vs*. RHE, and (c) the relative frequency of surface potential values before and after CV cycling.

## 6. Electrochemical characterization on Au-RDE

A series of CVs were carried out on $Ir/Ti_4O_7$ coated Au-RDEs in order to study the electrochemical surface reactions. Commercial Ir-black catalyst and $Ti_4O_7$ support were measured for comparison purposes. Fig. S5 (a), Fig. S5 (c) and Fig. S5 (e) show the resulting electrochemical characteristics, measured in Ar-saturated electrolyte solution, of Ir-black, $Ti_4O_7$ support, and $Ir/Ti_4O_7$, respectively. Likewise, the measurements performed in $O_2$-saturated electrolyte solution are presented in Fig. S5 (b), Fig. S5 (d), and Fig. S5 (f) for Ir-black, $Ti_4O_7$, and $Ir/Ti_4O_7$, respectively. The cycles were performed in the presence of oxygen and are in fact more representative of the anode of a PEM electrolyzer. As can be seen the characteristic triplets of adsorption ($H_{ads}$) of hydrogen on Ir-black appear in the potential window between 0.05 and 0.35 V *vs*. RHE [3]. The upper potential limit of 0.35 V *vs*. RHE corresponds to the hydrogen underpotential deposition ($H_{upd}$) on metallic Ir [4]. Furthermore, the potential window between 0.3 and 0.4 V *vs*. RHE

corresponds to the double layer charging window, which consists of the overlap of strongly bound $H_{ads}$ and the upd of $OH^-$ radicals. Also, two subsequent anodic plateaus centered at 0.67 and 0.96 V *vs.* RHE can be observed, which correspond to the formation of $Ir(OH)_3$ and hydrous $Ir^{4+}$ species, respectively [5]. Further increase of potential leads to the formation of $Ir^{5+}$ species on Ir-black, which cannot be reduced in the backwards scan. The formation of hydrous $IrO_x$/Ir gradually hinders the hydrogen adsorption in the cathodic region of the voltammogram. Consequently, the anodic and cathodic peaks decrease in intensity as the number of cycles is progressively increased, due to the formation of oxide species on the surface. On the other hand, the presence of oxygen in the electrolyte solution produces an overall negative shift of the anodic currents below 0.65 V *vs.* RHE, as a consequence of the oxygen reduction reaction (ORR) on Ir-black and the Au disc. The $H_{upd}$ and reduction of $Ir^{3+}$ are shifted to more negative potentials as well. Lastly, the formation $Ir^{n+}$ species in the oxidative environment is favored [5], leading to a more rapid decrease of $H_{ads}$ peaks intensity through the cycles.

Rather different electrochemical surface characteristics were obtained for the Magnéli phase $Ti_4O_7$ that is used as support of Ir nanoparticles. First, one can observe in Fig. S5 (c) that the $Ti_4O_7$ substrate remains almost entirely passive in the deaerated environment, between the lower and upper potential limits of the CV, as reported elsewhere. However, in the $O_2$-saturated electrolyte (Fig. S5 (d)) a concomitant cathodic wave in the negative potential region increases gradually in intensity as well as the starting potential, after each cycle. This reduction current density originates in the ORR at ca. 0.5 V *vs.* RHE on uncoated areas of Au disc of the RDE.[6] The reduction of $Au^{3+}$ at about 1.15 V also takes place within the chosen potential window of the CV. These highly active electrochemical reactions that occur beneath the $Ti_4O_7$ layer might contribute to the gradual detachment of the sample.

Fig. S5 (e) and Fig. S5 (f) show the cyclic voltammetric characteristics of the Ir/$Ti_4O_7$ catalyst developed in this work, performed in Ar- and $O_2$-saturated 0.5 M $H_2SO_4$. The differences in the electrochemical fingerprint of Ir/$Ti_4O_7$ and Ir-black are quite distinctive. Most of the surface reaction peaks and plateaus involving $H_{upd}$ an $Ir^{n+}$ species in Ir-black, are smoothed for Ir/$Ti_4O_7$. This feature gives account of the differences in morphology between the two catalysts in spite of the high degree of metallicity of both materials (see Section 3.1.3). Through the successive scans the maximum anodic and cathodic peaks decrease gradually due to the formation of $Ir^{5+}$ species that covers the surface of the Ir nanoparticles. One interesting feature in the cyclic voltammogram is the anodic wave that starts at 0.2 V *vs.* RHE. This reaction is not related to the adsorption of hydrogen species, but rather a reversible change on the oxidation states of Ti atoms at the electrode surface [7]. As it will be shown later this cathodic reaction does not have any negative effect in the OER activity of Ir/$Ti_4O_7$ in deaerated electrolyte solution, even after holding the potential constant at 0.05 V *vs* RHE.

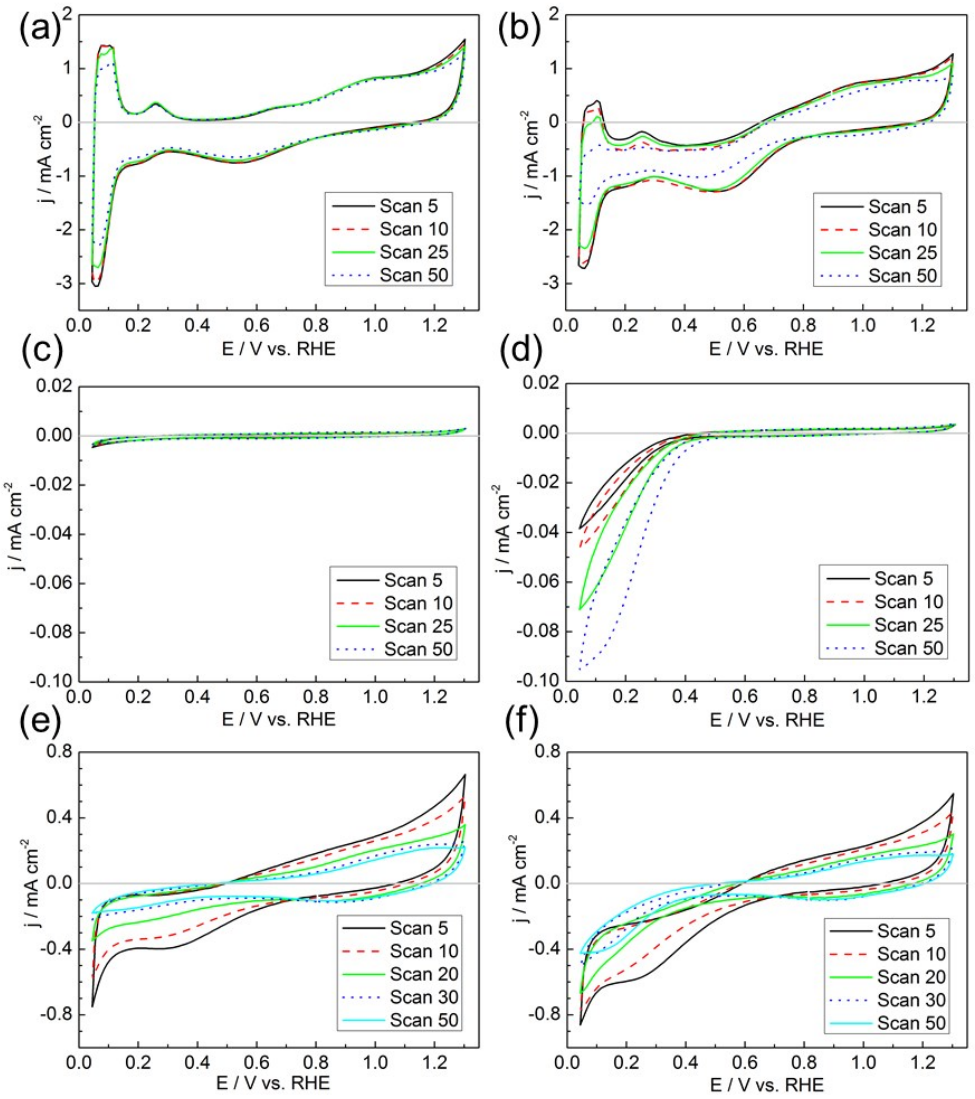


**Fig. S5.** Cyclic voltammetric characteristics measured in Ar-saturated 0.5 M $H_2SO_4$ on (a) Ir-black, (c) $Ti_4O_7$ and (e) Ir/$Ti_4O_7$ deposited on the Au-RDE. The corresponding measurements in $O_2$ -saturated 0.5 M $H_2SO_4$ are shown in (b), (d) and (f). Measurements were carried out at 100 mV $s^{-1}$ and 24 °C.

Similar effect observed on GC-RDE was corroborated using an Au-RDE and upholding the CVs up to 1.4 V *vs.* RHE to enhance the transition between oxide monolayer and thick-film state [3]. These measurements were carried out on Au-RDE as the surface influence from unstable $Au_2O_3$, normally formed at 1.46 V *vs.* RHE [6], is negligible in this case. The results are shown in Fig. S6 (a) and Fig. S6 (b) for Ir-black and Ir/$Ti_4O_7$, respectively.

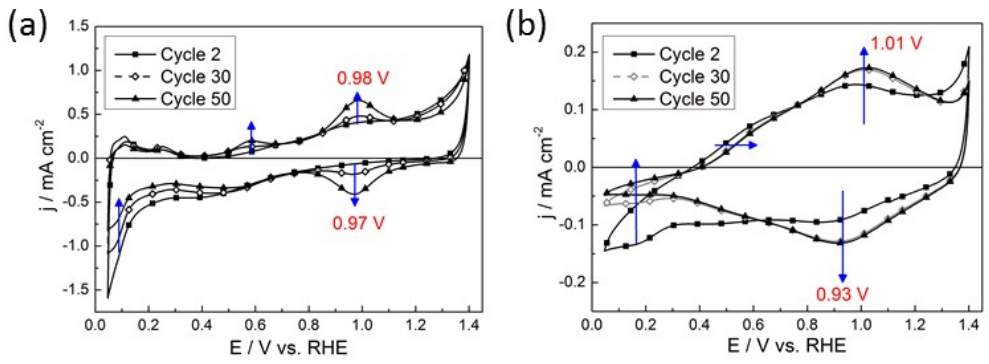


**Fig. S6.** Cyclic voltammetric curves of (a) Ir-black and (b) Ir/$Ti_4O_7$ on Au-RDE were carried out up to 1.4 V *vs.* RHE at a sweep rate of 50 mV $s^{-1}$.

## 7. CV comparison between commercial $IrO_2$ (Sigma Aldrich) and Ir/$Ti_4O_7$

In order to compare the difference of $Ir^{3+} \rightarrow Ir^{4+}$ peaks between commercial $IrO_2$ (Sigma Aldrich) and Ir/$Ti_4O_7$, 100 cycles CV with a scanning rate of 50 mV $s^{-1}$ were carried out on both samples from 0.05 V to 1.2 V vs. RHE, the 100$^{th}$ CV was used for comparison showed in Fig. S7. Commercial $IrO_2$ (Sigma Aldrich) showed $Ir^{4+}$ peak at around 0.8 V vs. RHE, which is consistent with the results Siracusano *et. al.* reported.[8] However, $Ir^{4+}$ peak for Ir/$Ti_4O_7$ was observed above 0.9 V vs. RHE, the $Ir^{3+} \rightarrow Ir^{4+}$ peak shifts to positive potential. In general, the $Ir^{3+} \rightarrow Ir^{4+}$ peak is centered at 0.8 V for thermally oxidized Ir, while for electrochemically oxidized Ir redox reaction takes place at higher potentials.[9-11]

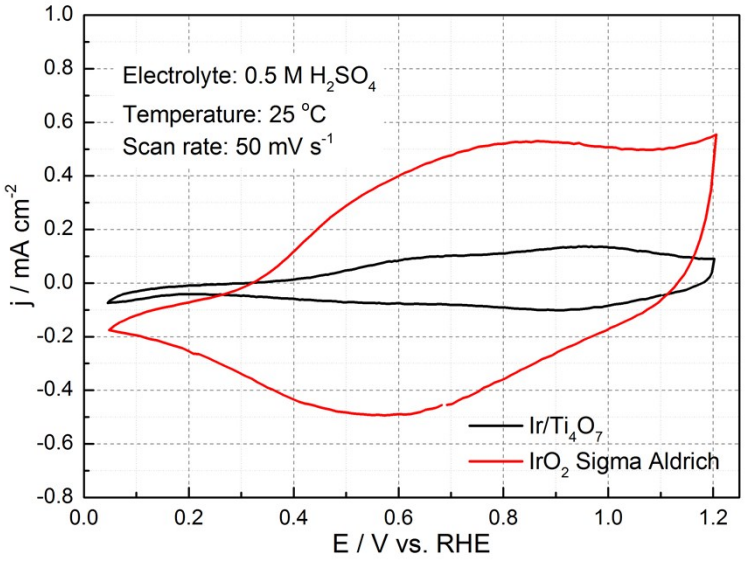


**Fig. S7.** The 100$^{th}$ scan CV comparison between Ir/$Ti_4O_7$ and commercial $IrO_2$ (Sigma Aldrich).

## 8. Accessible active sites determination (redox peak) and TOF calculation

In order to determine the active center numbers on Ir-based catalyst, $Ir^{3+} \leftrightarrow Ir^{4+}$ redox peak was used to estimate the accessible active sites for both catalysts as P. Strasser *et. al.* reported.[2] For this purpose, the charge of the oxidation peak from $Ir^{3+}$ to $Ir^{4+}$ was used considering the subtraction of the capacity current. The charge of the considered oxidation peak is a one electron reaction wherefore the division by electron charge brings out the number of active atoms, namely accessible active sites. The calculation details showed in Table S1.

**Table S1.** Accessible active sites calculation on Ir-black and $Ir/Ti_4O_7$

| | Ir-black | $Ir/Ti_4O_7$ |
|---|---|---|
| Active sites: mol / g | $5.72 \times 10^{-4}$ | $8.26 \times 10^{-5}$ |
| $Q/Q_e$: number of $e^-$ (number of active atoms) | $3.45 \times 10^{20}$ | $4.98 \times 10^{19}$ |
| $Q_e$ | $1.6 \times 10^{-19}$ | $1.6 \times 10^{-19}$ |
| Q in C/g | 55.24 | 7.98 |

The turnover frequency (TOF) was calculated by the following equation:

$$TOF = \frac{j\,[A\,g^{-1}]}{n \cdot Q\,[C\,g^{-1}]} \quad (1)$$

where n=4, considering that all the kinetic current is used for OER.

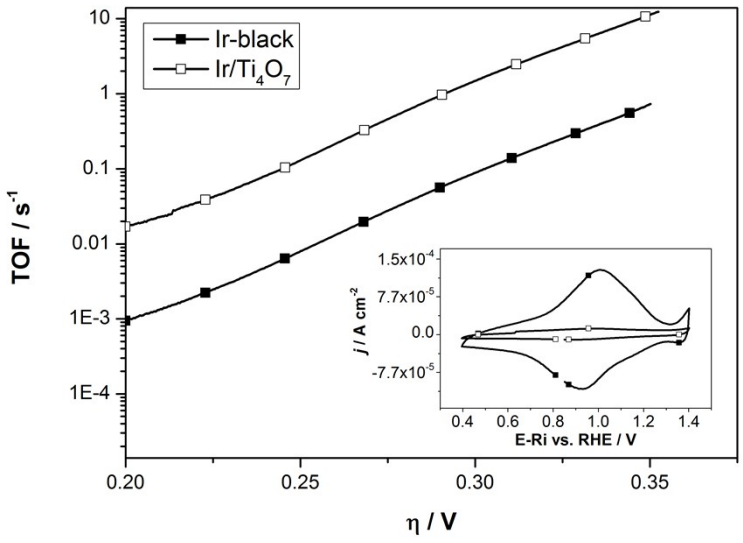


**Fig. S8.** TOF comparison between Ir-black and $Ir/Ti_4O_7$ along with overpotential increasing, the inset is the corresponding $Ir^{3+} \leftrightarrow Ir^{4+}$ redox peak for both catalysts.

## 9. Determination of electrochemically active sites by CO-stripping technique

Another strategy for studying the surface sites on PGM catalyst is by CO-stripping. The technique has been widely used for determining the number of active sites and studying the ad-

atom coverage rate phenomena on Pt [12,13] based catalysts. In the case of OER catalysts one can only determine the specific current densities rather than the electrochemically active surface area associated to the intrinsic OER activity.[14] In this study the potential is hold below the $H_{upd}$ for a certain period of time, thus the monolayers of hydrous $IrO_x$ are reduced to $Ir^0$ which subsequently adsorbs the CO molecules ($CO_{ads}$). From the current transient at 0.05 V *vs.* RHE shown in Fig. S9 (a), one can observe that both catalysts became poisoned with CO molecules after less than 100 s reaching a steady state. The cathodic current density of $Ir/Ti_4O_7$ is slightly higher than Ir-black since the ceramic support also contributes to the cathodic current at this potential. Thereafter, three CVs with a scanning rate of 50 mV $s^{-1}$ and in Ar-saturated 0.5 M $H_2SO_4$ are performed from 0.05 to 1.2 V *vs.* RHE in order to oxidize the $CO_{ads}$ on $Ir^0$ to molecular $CO_2$. The results for the Ir-black and $Ir/Ti_4O_7$ catalysts are shown in Fig. S9 (b) and (c), respectively. The OER activities, shown in the inset of the Figures, were measured before and after the CO-stripping. In both cases the measured current density at any overpotential increases slightly after the CV. This effect can be due to the $Ir^{4+}$ oxide layer formation, which is porous and provides access to the underlying non oxidized Ir.

The surface (S) of CO oxidation peak was used to determine the electrochemically active sites of catalysts.

$$S = A \cdot V = \frac{Q}{s} \cdot V = Q \cdot \frac{V}{s} \quad (2)$$

in which, $S$ is the surface integrated from the plot, $A$ is current, $V$ is potential, $Q$ is the electric charge of CO oxidation, $s$ is time. $V$ is scanning rate used in the experiments.

Thus,

$$Q = \frac{S}{V/s} \quad (3)$$

Where, Q means the electric charges which were needed for all the adsorbed CO molecules to be oxidized to $CO_2$. Here, for each electrochemically active site of the catalysts, it was assumed to be occupied by a single CO molecule, and two electrons were needed when CO was oxidized to $CO_2$. Therefore, the number of all adsorbed CO molecules equals to the number of the active sites of the catalyst on GC electrode, namely:

$$N_{active\ sites} = N_{CO} = \frac{Q/Q_{e^-}}{2} \quad (4)$$

By integrating the charge of the CO oxidation peaks, it was calculated to be $4.04 \times 10^{-4}$ mol $g_{Ir}^{-1}$ and $1.68 \times 10^{-4}$ mol $g_{Ir}^{-1}$ for Ir-black and $Ir/Ti_4O_7$, respectively. Remarkably, the normalized surface sites of the unsupported catalyst are ca. 2.4 times than the supported one, although the mass activities follow the opposite trend.

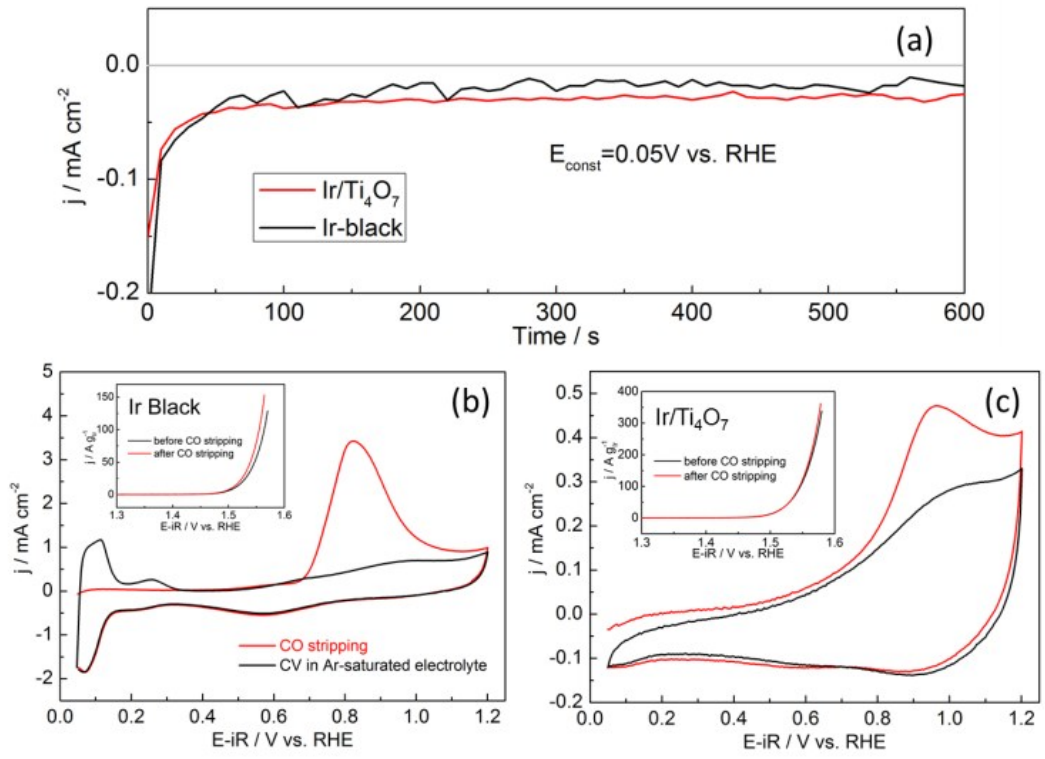


**Fig. S9.** CO-stripping (a) current transients at 0.05 v *vs.*RHE and cyclic voltammetric curves of (b) Ir-black and (c) Ir/$Ti_4O_7$ catalysts, which were carried out at a sweep rates of 50 mV $s^{-1}$ in 0.5 M $H_2SO_4$ electrolyte. The insets in (b), (c) show the corresponding OER mass activity characteristics before and after the electrochemical cycling with a 5 mV $s^{-1}$ scan rate and 2500 rpm rotation speed.

## 10. pH measurements

Table S2 summarizes the pH of $Ti_4O_7$, $TiO_2$, Ir-black and Ir/$Ti_4O_7$ deionized water suspensions. Measurements were carried on three different suspensions of each powder.

**Table S2.** pH values of $Ti_4O_7$, $TiO_2$, Ir black and Ir/$Ti_4O_7$

| Sample | Suspension [1 mg/ml] | pH | Averaged pH | T [°C][a] |
|---|---|---|---|---|
| $Ti_4O_7$ | No. 1 | 9.1 | 9.1 | 25.8 |
| | No. 2 | 9.2 | | 26.0 |
| | No. 3 | 9.2 | | 26.0 |
| $TiO_2$ | No. 1 | 6.6 | 6.2 | 26.7 |
| | No. 2 | 6.1 | | 26.1 |
| | No. 3 | 6.1 | | 25.7 |
| Ir-black | No. 1 | 6.1 | 6 | 26.7 |
| | No. 2 | 6 | | 25.8 |
| | No. 3 | 6 | | 26.6 |

| | | | | |
|---|---|---|---|---|
| $Ir/Ti_4O_7$ | No. 1 | 5.7 | 5.8 | 26.1 |
| | No. 2 | 5.7/5.9[b] | | 26.2/25.1 |
| | No. 3[c] | 6.7 | | 25.9 |

[a] T means the suspension temperature when the pH value was read.
[b] Suspension No. 2 of $Ir/Ti_4O_7$ was measured twice independently.
[c] Suspension No. 3 was prepared by the catalyst pellet which was used for AFM measurements before, this could be the reason why the pH value is higher than suspension No. 1 and suspension No. 2. Therefore, this value was not used for averaging the pH.

## 11. Zeta potential measurements

The Zeta potentials of $Ti_4O_7$, Ir black and $TiO_2$ (Sigma-Aldrich, No. 634662, < 100 nm particle size) are measured and the results showed in Fig. S11. In the case of $Ti_4O_7$, ca. -120 mV was observed, it demonstrated an excellent stability of $Ti_4O_7$ when the particles were dispersed in deionized water. On the other hand, negative Zeta potential displays that the $Ti_4O_7$ particle surface was surrounded by negative charge in suspension, which is consistent with pH value measurements.

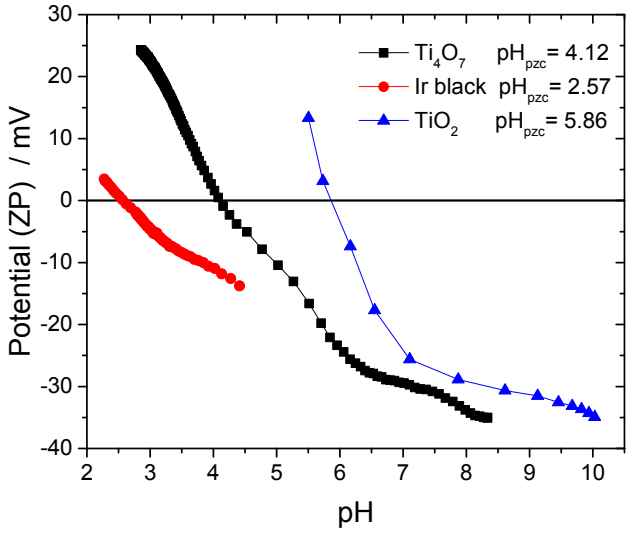


**Fig. S10.** Measurement of the point of zero charge ($pH_{PZC}$) for $Ti_4O_7$, Ir black and $TiO_2$ by titration. The determined $pH_{PZC}$ are given in the diagram.

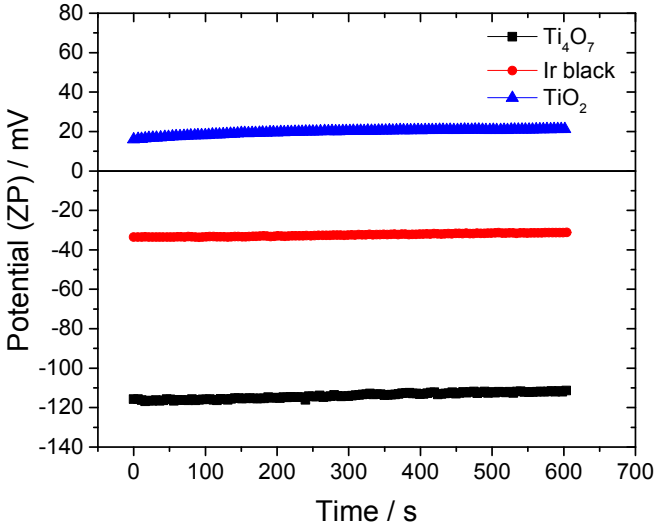


**Fig. S11.** Measurement of the suspensions at their pH in water for $Ti_4O_7$, Ir black and $TiO_2$.

## 12. Ir content determination by EDX

In order to more exactly determine the Ir content in the Ir/$Ti_4O_7$ sample, EDX technique was used with two different ways for sample preparation.

First method

Ir/$Ti_4O_7$ powders (as-prepared) were dispersed manually by technician on a conductive carbon tape without any further press, then six areas with different sizes (max. ca. 100 µm x 40 µm) were analyzed by EDX for Ir content determination. The results showed in Table S3 at the end, the Ir content of 25.8 wt. % was achieved by averaging 6 values out of all the tested areas. The calculated standard deviation is 4.3 wt%. Therefore, Ir content of Ir/$Ti_4O_7$ was determined as 25.8 ± 4.3 wt.%.

**Table S3.** Element content of Ir/$Ti_4O_7$ analyzed by EDX with dispersed sample

| Analyzed area (different sizes) | C/ wt.% | O/ wt.% | Cl/ wt.% | K/ wt.% | Ti/ wt.% | Ir/ wt.% |
|---|---|---|---|---|---|---|
| DLR1 | 5.77 | 20.37 | 7.34 | 0.70 | 40.45 | 25.4 |
| DLR2 | 4.11 | 14.58 | 7.17 | 0.64 | 44.20 | 29.3 |
| DLR3 | 5.94 | 27.72 | 5.28 | 0.52 | 40.30 | 20.2 |
| DLR4 | 5.49 | 22.92 | 4.54 | 0.35 | 34.87 | 31.8 |
| DLR5 | 5.89 | 15.69 | 8.26 | 0.45 | 42.37 | 27.3 |
| DLR6 | 8.66 | 25.00 | 5.13 | 0.57 | 40.16 | 20.5 |
| Average | | | | | | 25.8 |

Second method

$Ir/Ti_4O_7$ powders (as-prepared) were pressed on the gold plate forming a compressed pellet. Then the gold plate with sample was analyzed. From the surface of sample pellet, eight independent areas, 190 μm × 140 μm for each, were selected and analyzed by EDX for Ir content, the results showed in Table S4. The final Ir content, 24.2 wt. %, was obtained from the average of the eight areas, with a standard deviation of 0.8 wt. %. The EDX detector is able to provide an accuracy of ca. 0.4 wt%. Therefore, Ir content of $Ir/Ti_4O_7$ was determined 24.2 ± 0.8 wt.%.

**Table S4.** Element content of $Ir/Ti_4O_7$ analyzed by EDX on the compressed sample

| Analyzed area (190 μm × 140 μm) | C/ wt.% | O/ wt.% | Cl/ wt.% | K/ wt.% | Ti/ wt.% | Ir/ wt.% |
|---|---|---|---|---|---|---|
| A1 | N/A | 29.2 | 6.6 | 0.7 | 39.6 | 23.9 |
| A2 | N/A | 29.5 | 6.7 | 0.8 | 39.0 | 24.1 |
| A3 | N/A | 29.4 | 6.3 | 0.9 | 39.9 | 23.5 |
| A4 | N/A | 28.7 | 6.9 | 0.7 | 39.0 | 24.8 |
| A5 | N/A | 29.3 | 6.6 | 0.7 | 39.5 | 23.9 |
| A6 | N/A | 27.9 | 7.1 | 0.7 | 39.5 | 24.9 |
| A7 | N/A | 27.7 | 6.8 | 0.8 | 39.3 | 25.4 |
| A8 | N/A | 31.0 | 6.2 | 0.7 | 39.1 | 23.0 |
| Average | | | | | | 24.2 |

Both methods showed the similar mean Ir content values, however, the value determined by the second method was adopted in the manuscript since it has less error.

## References:


1 C. P. P. De Pauli and S. Trasatti, *J. Electroanal. Chem.*, 1995, **396**, 161–168.
2 H. N. Nong, L. Gan, E. Willinger, D. Teschner and P. Strasser, *Chem. Sci.*, 2014, **5**, 2955.
3 J. Mozota and B. E. E. Conway, *Electrochim. Acta*, 1983, **28**, 1–8.
4 J. Durst, C. Simon, F. Hasche and H. a. Gasteiger, *J. Electrochem. Soc.*, 2014, **162**, F190–F203.
5 J. Juodkazytė, B. Šebeka, I. Valsiunas and K. Juodkazis, *Electroanalysis*, 2005, **17**, 947–952.
6 L. D. Burke and P. F. Nugent, *Gold Bull*, 1997, **30**, 43–53.
7 J. R. Smith, F. C. Walsh and R. L. Clarke, *J. Appl. Electrochem.*, 1998, **28**, 1021–1033.
8 S. Siracusano, V. Baglio, C. D'Urso, V. Antonucci and A. S. Aricò, *Electrochim. Acta*, 2009, **54**, 6292–6299.
9 T. Reier, M. Oezaslan and P. Strasser, *ACS Catal.*, 2012, **2**, 1765–1772.
10 D. A. J. Rand and R. Woods, *J. Electroanal. Chem. Interfacial Electrochem.*, 1974, **55**, 375–381.
11 S. Gottesfeld and S. Srinivasan, *J. Electroanal. Chem. Interfacial Electrochem.*, 1978, 86, 89–104.
12 F. Maillard, M. Eikerling, O. V. Cherstiouk, S. Schreier, E. Savinova and U. Stimming, *Faraday Discuss.*, 2004, **125**, 357.
13 K.A. Friedrich, F. Henglein, U. Stimming and W. Unkauf, *Electrochim. Acta*, 2000, **45**, 3283–3293.

14 T. Reier, M. Oezaslan and P. Strasser, *ACS Catal.*, 2012, **2**, 1765–1772.